OPEN ACCESS

University of BRISTOL

Goulianos, A., Yuan, W., Berkovskyy, D., Charitos, M., & Armour, S. (2016). Large-Scale Modeling and Cell-edge Coverage for Future HetNet Deployments. In *2016 IEEE 83rd Vehicular Technology Conference (VTC Spring 2016): Proceedings of a meeting held 15-18 May 2016, Nanjing, China* (pp. 1180-1184). Institute of Electrical and Electronics Engineers (IEEE). https://doi.org/10.1109/VTCSpring.2016.7504317

Peer reviewed version

Link to published version (if available):
10.1109/VTCSpring.2016.7504317

Link to publication record in Explore Bristol Research
PDF-document

This is the author accepted manuscript (AAM). The final published version (version of record) is available online via IEEE at http://ieeexplore.ieee.org/document/7504317/. Please refer to any applicable terms of use of the publisher.

University of Bristol - Explore Bristol Research
General rights

This document is made available in accordance with publisher policies. Please cite only the published version using the reference above. Full terms of use are available:
http://www.bristol.ac.uk/red/research-policy/pure/user-guides/ebr-terms/

Large-Scale Modeling and Cell-edge Coverage for Future HetNet Deployments

Angelos A. Goulianos, Wenfang Yuan , Denys Berkovskyy, Michael Charitos and Simon Armour

Communication Systems & Networks Group
University of Bristol, Merchant Venturers Building, Woodland Road, Bristol BS8 1UB, UK
Email: {a.goulianos, wy12292, Simon.Armour}@bristol.ac.uk

***Abstract*— This paper evaluates the large-scale channel parameters and the cell-edge coverage for various LTE-WiFi based, heterogeneous networks. Real world urban databases are incorporated into two separate 3D ray tracing software tools, specifically designed for the characterization of both microwave and millimeter (mm)-wave radio links. The study is performed for both LTE-800MHz and LTE-2.6GHz macro-cell configurations whereas it demonstrates the coverage enhancement attained by deploying 802.11n/ac/ad micro-cell structures. The significance of this study lies on the radio planning aspects of future heterogeneous networks.**

Keywords—Heterogeneous Networks; WiFi; LTE; Macro-cells, Pico-cells, ray tracing.

I. INTRODUCTION

The remarkable increase of mobile broadband data traffics follows an exponential growth at a compound rate of 108%. This growing demand gives rise to a capacity challenge with an estimated average increase of 29% per year [1]. LTE-Advance offers a promising energy efficient solution to increase cellular capacity that could potentially offload the high power and expensive macro-cell Base Stations (BSs). This can be achieved through the deployment of low-power macro/femto relay BSs in the so-called Heterogeneous Networks (HetNets) configurations.

Several recent studies have investigated the enhanced coverage and throughput performance of joint macro-pico-cell networks. However, most of the available work focuses on LTE based HetNets [2] or on macro-relay networks [3].

To the best of the authors' knowledge, there is no existing study in literature that characterizes the large-scale parameters and cell-edge coverage with respect to different outdoor pico and macro-cell deployments. To address this issue, the presented work provides an enhanced study on the signal degradation of various macro and pico-cell scenarios. More specifically, LTE-800MHz and LTE-2.6GHz are considered for the case of macro-cell study. For the pico-cell deployment 802.11n, 802.11ac and 802.11ad systems are investigated. It is important to mention that the presented study was based on realistic channel matrices generated with the aid of advanced 3-D ray-tracing tools developed by the University of Bristol, UK.

The remainder of this paper is organized as follows: Section II provides a comprehensive overview of the channel generation process and the antennas configuration for microwave and mm-wave links. In Section III, the modeling methodology that is followed for the macro-cell deployments is provided. Section IV presents the corresponding results for the micro-cell configurations. Finally, Section V presents key conclusions drawn from this work.

II. CHANNEL GENERATION AND ANTENNAS CONFIGURATION

A. Channel Generation for Microwave Links

The spatial and temporal multipath components of the propagation channel between each base station (BS) and user location are modelled using a 3 dimensional (3-D) outdoor ray-tracing tool developed at the University of Bristol. The same tool has been successfully used in previous studies for the modelling of various propagation environments [4].

Point-source ray tracing provides information on the amplitude, phase, time delay, azimuth and elevation Angle of Departure (AoD) and Angle of Arrival (AoA) of each multipath component (MPC). The complex gain of each MPC were adjusted according to the transmitting and receiving antenna electric field pattern response for the corresponding AoD/AoA and polarisation. The generalized expression for the double-directional time-variant channel impulse response h for a dynamic channel link is given by [5]:

$$\begin{aligned} &h(t,\tau,\Omega_{AoD},\Omega_{AoA}) \\ &= \sum_{l=1}^{L} h_l(t,\tau,\Omega_{AoD},\Omega_{AoA}) \\ &= \sum_{l=1}^{L} \mathbf{E}_l(t)\delta(\tau-\tau_l)\delta\left(\Omega_{AoD}-\Omega_{AoD,l}\right)\delta\left(\Omega_{AoA}-\Omega_{AoA,l}\right) \end{aligned} \quad (1)$$

where,

$$\boldsymbol{E_l}(t) = \begin{bmatrix} E_{Tx}^{V} \\ E_{Tx}^{H} \end{bmatrix}^{T} \begin{bmatrix} a_l^{VV} e^{j\varphi_l^{VV}} & a_l^{VH} e^{j\varphi_l^{VH}} \\ a_l^{HV} e^{j\varphi_l^{HV}} & a_l^{HH} e^{j\varphi_l^{HH}} \end{bmatrix} \begin{bmatrix} E_{Rx}^{V} \\ E_{Rx}^{H} \end{bmatrix} e^{j2\pi\upsilon_l t} \quad (2)$$

In the above equation, $\delta(\cdot)$ represents the Dirac delta function, t is elapsed time, τ is the time-of-flight, $\Omega_{AoD}/\Omega_{AoA}$ represent the departure/arrival solid angles and L is the total number of MPCs. The l^{th} MPC is represented by h_l, which includes complex amplitude $a_l^{XY} e^{j\varphi_l^{XY}}$ (2x2 matrix for all four polarisation combinations), time-of-flight τ_l, Doppler shift υ_l

978-1-5090-1698-3/16/$31.00 ©2016 IEEE

and departure/arrival solid angles $\Omega_{AoD,l}/\Omega_{AoA,l}$. $E_{Tx}^{V/H}/E_{Rx}^{V/H}$ represent the vertical/horizontal polarisation components of the transmitting and the receiving antenna electric field radiation patterns. For the purpose of signal prediction, static channels are only assumed, and therefore the Doppler phase term in Eq. 2 is set to zero.

Two types of antennas are considered for the case of microwave Het-Net links. It is assumed that for the Wi-Fi and the 802.11ac pico-cell study, both the transmitter and the receiver are modelled with a theoretical omni-directional vertical Hertzian dipole having a directivity of 1.8dBi. For the case of LTE cells, the base-stations are equipped with a 3-sector directional antenna array of 10 slant patch elements down-tilted by 10^0. The antennas for both LTE-800MHz and LTE-2.6GHz have been measured in the University of Bristol's anechoic chamber and have a directivity of 13 dBi.

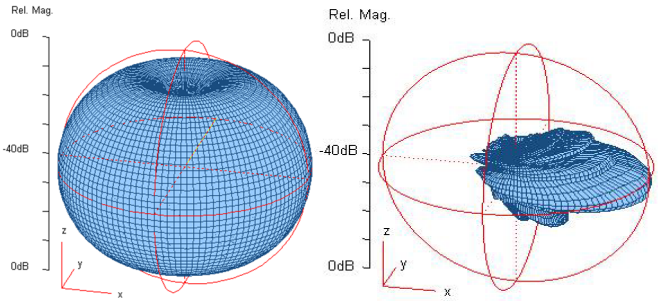

(a) (b)

Figure 1. 3-D antenna radiation patterns. (a) Vertical Hertzian dipole; (b) LTE Base Station antenna.

On the other hand, at the receiver side, the users are assumed to employ the same omni-directional antennas as in the case of Wi-Fi systems. The antennas patterns employed for the case of microwave links are illustrated in Fig. 1.

B. Channel Generation for mm-wave Links

To have an insight of the outdoor mm-wave cellular systems, a 3D ray tracing tool has also been developed for the case of 60 GHz transmissions. The model is a modified version of the indoor channel model proposed by IEEE 802.11ad channel for 60 GHz WLANs [6]. Taking into consideration the reflection loss and foliage attenuation, the outdoor ray-tracing provides accurate temporal and spatial information of significant paths, including the direct link, as well as the first and second order reflections from building walls, between each base-station and user location.

The signal strength is attenuated due to reflections from building walls. Instead of employing the statistical model provided in [6], the reflection loss for the case of perpendicular polarized transmissions is predicted by the following expression [7]:

$$PL_{\text{Reflection}} = \frac{\cos\theta_o - \sqrt{\varpi_o - (\sin\theta_o)^2}}{\cos\theta_o + \sqrt{\varpi_o - (\sin\theta_o)^2}} \quad (3)$$

The present study was funded by the EPSRC grant on: "Seamless and Adaptive Wireless Access for Efficient Future Networks." (SERAN).

where θ_o is the incident angle and ϖ_o denotes the dielectric constant, the value of which is set as $6.5 - 0.7j$ for concrete structure [7]. Furthermore, the signal attenuation due to foliage is given by:

$$PL_{\text{Foliage}}[\text{dB}] = 0.2 \times (f_c)^{0.3} \times (d)^{0.6} \quad (4)$$

where f_c is the central frequency and d is the depth of foliage in meters [8].

To compensate for the large propagation loss in mm-wave channels, a uniform linear array with 32 antennas is employed at the BS to perform a codebook-based beamforming (BF). The codebook design considered in this paper is based on the proposed codebook provided in [9], and is specified by an $M \times K$ matrix W:

$$W(m,k) = j^{floor\{\frac{m \times mod(k+(K/2),K)}{K/4}\}},$$
$$m = 0, \cdots M-1;\ k = 0, \cdots, K-1; \quad (5)$$

where M is the number of antennas and K is the number of feasible beams. The function $floor(x)$ returns the biggest integer smaller than or equal to x and function $mod(x,y)$ is $x - n \times y$ with $n = floor(x/y)$. The array factor for the $k-th$ column vector of the codebook matrix W is:

$$AF_k(\varphi) = \sum_{m=0}^{M-1} W(m,k) e^{j2\pi m(d/\lambda)\sin(\phi)} \quad (6)$$

where λ is the wavelength and d is the antenna separation. ϕ denotes the polar angle in respect of $x-$axis, given that antennas lie along $y-$axis. Fig. 2 illustrates the beam patterns created using the above mentioned codebook with $M = 32$ and $K = 64$.

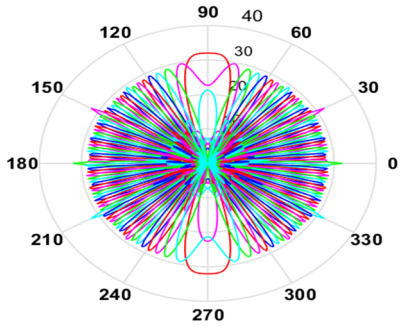

Figure 2. Beam patterns created using the codebook proposed in [3] with $M = 32$ and $K = 64$.

III. Macro-cell Modeling and Coverage Prediction

For the case of macro-cell study, both LTE-800MHz and LTE-2.6GHz have been considered. More specifically, 20 BSs were randomly placed in realistic locations within a 4x4Km ray-tracing map of the city of Bristol, UK. The height of the BS antennas was set at 30 m above the ground level, and the transmit power was set to 45 dBm, which is well below the OfCom (Office of Communications, UK) regulations [10].

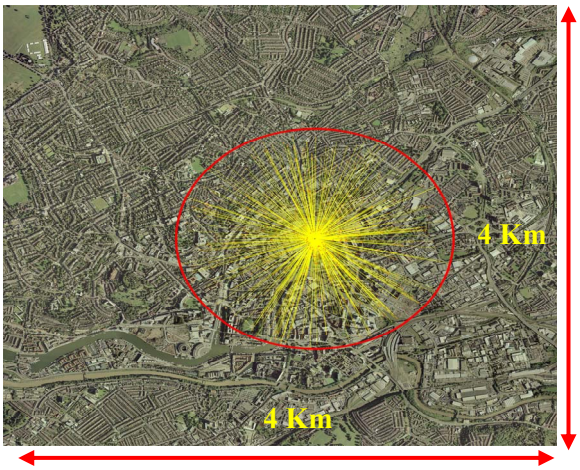

Figure 3. An exemplary LTE-800MHz macro-cell scenario.

For each of the base stations, 1000 User Equipment (UE) locations were randomly chosen within a radius of 1 Km from the BS. The UE terminal height was set to 1.5 m above the ground level. Therefore, 20000 links were simulated in total for each macro-cell scenario. Various exemplary BS to UE link scenarios for LTE-800MHz s are illustrated in Fig. 3.

To characterize the path-loss trend from the measured data, the well-known linear regression model was employed [11]:

$$PL(d) = P_0 + 10nlog_{10}\left(\frac{d}{d_0}\right) + X_\sigma \qquad (7)$$

where $PL(d)$ is the link-loss (in dB) at a distance d from the BS, P_0 denotes the reference path-loss at a distance d_0, which was 50m for LTE macro-cells, n is the path-loss exponent and X_σ is the shadowing term , which is a zero-mean Gaussian distributed random variable with standard deviation σ. Both X_σ and σ are expressed in dB units. The results for the path-loss evaluation of LTE-800MHz and LTE-2.6GHz are depicted in Fig. 4 and Fig. 5 respectively.

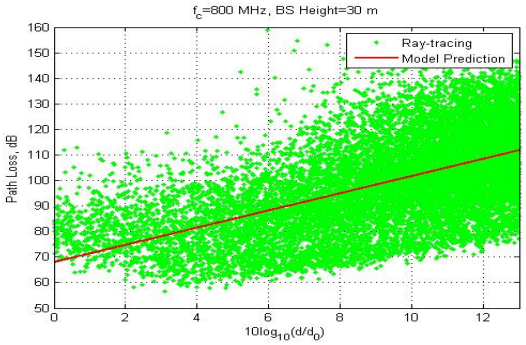

Figure 4. Ray-tracing data and model prediction for LTE-800MHz.

The shadowing term was found to have an approximately constant value with distance for both LTE macro-cell scenarios. This becomes apparent from Fig. 6 where the variation of shadowing with respect to the UE distance from the BS is illustrated.

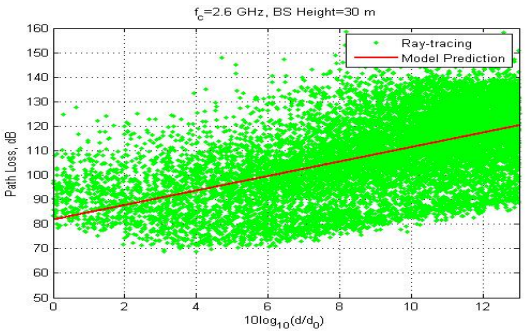

Figure 5. Ray-tracing data and model prediction for LTE-2.6GHz.

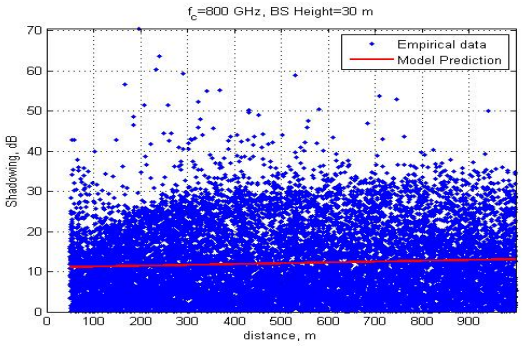

Figure 6. Shadowing plot with respect to distance for LTE macro-cells.

The predicted channel parameters are summarized in Table I. These metrics can be used in order to evaluate the probability that the received signal will exceed a particular level. In the presented study this level represents the receiver sensitivity R_S and was set to -95 dBm.

The probability that the received signal P_r will exceed R_S (outage) is given by the following expression:

$$p(P_r(d) \geq R_S) = Q\left(\frac{R_s - P_r(d)}{\sigma}\right) \qquad (8)$$

Combining Eq. 7 and Eq. 8 the resulting probability is given by:

$$p(P_r(d) \geq R_S) = Q\left(\frac{R_s - \left[P_t - P_0 - 10nlog\left(\frac{d}{d_0}\right)\right]}{\sigma}\right) \qquad (9)$$

where P_t denotes the transmitted power and $Q(x)$ returns the Q function of the argument x. Please, note that $PL(d)$ and P_t are related as follows:

$$P_r(d) = P_t - PL(d) \qquad (10)$$

TABLE I. LARGE -SCALE PARAMETERS AND COVERAGE FOR LTE MACROCELLS

Macrocell Scenario	Path-loss exponent (n)	Reference distance d_0(m)	σ (dB)	Coverage (m)
LTE-800MHz	3.3	50	11	1150
LTE-2.6GHz	2.9	50	11.4	560

The coverage shown in Table I, is the solution of Eq. 9 with respect to distance for 99% outage.

IV. PICOCELL MODELING AND COVERAGE PREDICTION

For the the pico-cell study, the 802.11n, 802.11ac and 802.11ad standards are investigated. The central frequencies used for the ray-tracing simulations were 2.4 GHz, 5.25 GHz and 60 GHz respectively. In the remainder of this section, the large-scale and coverage parameters are provided for the presented pico-cell scenarios.

A. Evaluation of 802.11n and 802.11ac pico-cells

For the case of 802.11n study, 200 BSs have been randomly placed within the Bristol ray-tracing database. Following similar pico-cell studies [2], the height of the BS antennas was set at 5 m above the ground, whereas the UE height was at 1.5 m. Furthermore, the transmitted power was at 20 dBm and the receiver sensitivity was set to -95 dBm. A total of 20000 profiles were created for the purpose of the 802.11n propagation study. For all the pico-cells scenarios the reference distance d_0 was set to 5m.

Exemplary pico-cells within the Bristol map, as well as the links among the BSs and the user terminals, are illustrated in Fig. 7.

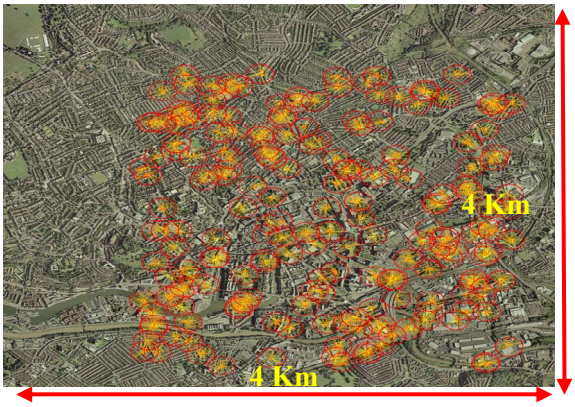

Figure 7. Wi-Fi simulated pico-cells within the Bristol database.

The large-scale and coverage parameters for the 2.4 GHz links were modeled following the procedure described in the previous section. The simulated results for the purpose of path-loss evaluation, as well as the distribution of shadowing with respect to distance are illustrated in Fig. 8 and Fig. 9 respectively.

An interesting feature which is revealed in Fig. 9 is that in the case of Wi-Fi pico-cells scenarios, the shadowing increases with distance in a linear mode. As it will be shown in the next paragraphs, this is a common characteristic for all types of pico-cells considered in this study.

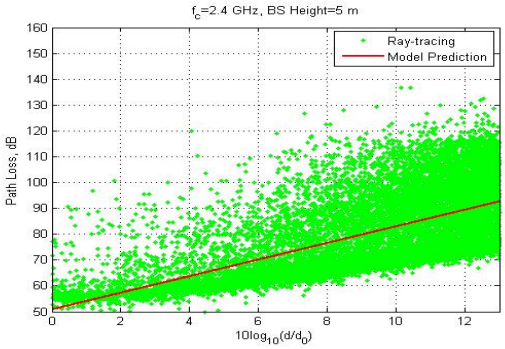

Figure 8. Path-loss with respect to distance for 802.11n pico-cells.

The physical insight behind this finding is that a low antenna height influences the variation of signal loss around its mean value. More specifically, at shorter distances the surrounding structures have less of an impact in the direct link transmission between the BS and the UE. On the other hand, as the UE moves away from the transmitter range, the contribution of the surrounding scatterers becomes more significant.

In the case of macro-cell propagation the antenna height implies a constant impact of the surrounding scatterers in the received signal, since the macro-cell BS illuminates the cell area.

For the 802.11ac study, the set-up was similar to the one used for the 802.11n pico-cells. Fig. 10 illustrates the simulated results and the model prediction for 802.11ac pico-cells. A similar behavior with the 802.11n study, is obtained for the variation of shadowing with distance.

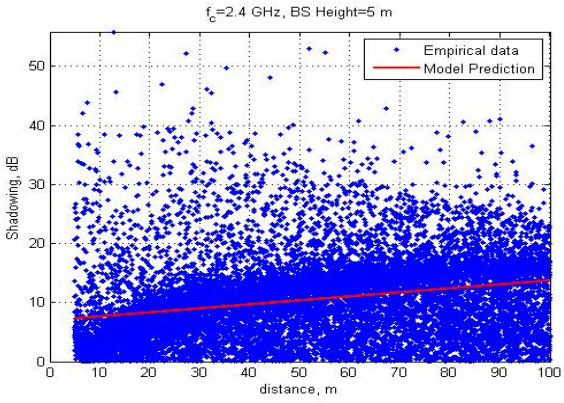

Figure 9. Shadowing plot with respect to distance for 802.11n pico-cells.

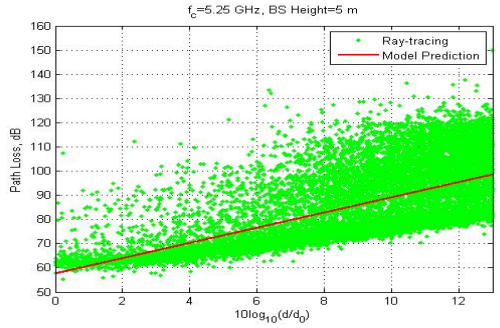

Figure 10. Path-loss with respect to distance for 802.11ac pico-cells.

B. Evaluation of mm-wave pico-cells

For the mm-wave pico-cell study, 20000 links have been generated within the Bristol data base, using a 3-D ray-tracing software, specifically developed for the purpose of modeling mm-wave propagation. The transmitted Effective Isotropic Radiated Power follows the regulations referred in [9] and was adjusted accordingly at the maximum value of 51.8 dBi. The results for the link path-loss and shadowing with respect to distance are depicted in Fig. 11.

It is apparent from the above figure, that the (BF) gain is approximately 30 dB when compared to the non-BF (NBF) case. Furthermore, BF has a significant impact in the pico-cell coverage distance. A summary of the large-scale parameters as well as the cell-edge coverage for all the pico-cell types considered in this study, is demonstrated in Table II.

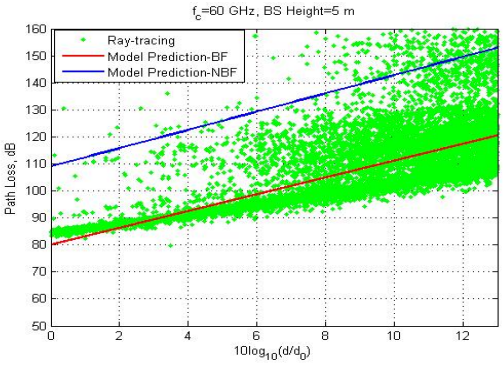

Figure 11. Path-loss with respect to distance for mm-wave pico-cells.

TABLE II. LARGE -SCALE PARAMETERS AND COVERAGE FOR PICO-CELL SCENARIOS

Pico-cell Scenario	$P_0(dB)$	**Path-loss exponent (n)**	σ **(dB)**	**Coverage (m)**
802.11n	50.9	3.2	$6.9 + 0.06d$	75
802.11ac	57.7	3.1	$6.7 + 0.07d$	60
802.11ad (BF)	80.1	3.1	$3.2 + 0.1d$	30

V. CONCLUSIONS

This paper provides large-scale models and cell-edge coverage results for various macro/pico-cell HetNet deployments. LTE-800MHz and LTE-2.6GHz were used as the macro-cell BSs whereas 802.11n, 802.ac and 802.11ad have been employed for the pico-cell study.

Results indicate that for the case of pico-cells, shadowing is linearly dependent on distance while no significant dependency was observed for the case of macro-cell configurations. Furthermore, assuming 99% reliability, the coverage enhancement provided by pico-cell-deployments is 75, 60 and 30m for the aforementioned WiFi standards.

Future work will extend this study by incorporating realistic channel matrices into appropriate system-level simulators for the purpose of performance evaluation of future HetNet architectures.

REFERENCES

[1] C. Khirallah, J.S.Thompson, " Energy and cost impacts of relay and femtocell deployments in long-term-evolution advanced", in IET Commun., Vol. 5, pp. 2617-2628, 2011.

[2] E.Mellios, G. Hilton and A.Nix, "Ray-tracing urban picocell 3D propagation statistics for LTE Heterogeneous Networks", in 7th European Conf. on Ant. and Propag., Gothenburg, 2013

[3] T. Beniero, et. al, "Effect of Relaying on Coverage in 3GPP LTE-Advanced", in Proc. VTC-Spring Conf, Barcelona, 2009.

[4] Yan Q. Bian, et al "MIMO–OFDM WLAN Architectures, Area Coverage, and Link Adaptation for Urban Hotspots", IEEE. Trans. on Vehic. Comm., vol. 57, no. 4, pp.2364-2374, 2008.

[5] M. Steinbauer, A. Molisch and E. Bonek, "The double-directional radio channel," IEEE Ant. and Propagat. Magazine, vol. 43, no. 4, pp. 51-63, Aug 2001.

[6] IEEE 802.11ad Channel Models for 60 GHz WLAN Systems, [Online]:Available: http://www.ieee802.org/11/Reports/tgad_update.htm

[7] X. An, et al, "Beam switching support to resolve link blockage problem in 60 GHz WPANs," in Proc. IEEE International Symposium on Personal Indoor and Mobile Radio Communications, pp. 390–394, Sep. 2009.

[8] CCIR, "Influences of terrain irregularities and vegetation on troposphere propagation," CCIR Report, 235–236, Geneva, 1986.

[9] "Wireless Medium Access Control (MAC) and Physical Layer (PHY) Specifications for High Rate Wireless Personal Area Networks (WPANs), Amendement 2: Millimeter-Wave-Based Alternative Physical Layer Extension, IEEE Standard 802.15.3c," Oct 2009.

[10] OfCom: "Consultation and Information on technical licence conditions for 800 MHz and 2.6 GHz spectrum and related matters", *Ofcom Official Document*, June 2nd , 2011.

[11] T. S. Rappaport, "Wireless Communications, Principles and Practice",Prentice Hall Inc., 2002.